Analytical and Bioanalytical Chemistry (2019) 411:6535–6547
https://doi.org/10.1007/s00216-019-01977-x

TRENDS

Microfluidic sample delivery for serial crystallography using XFELs

Austin Echelmeier[1,2] · Mukul Sonker[1,2] · Alexandra Ros[1,2]

Received: 16 April 2019 / Revised: 23 May 2019 / Accepted: 12 June 2019 / Published online: 27 June 2019

Abstract

Serial femtosecond crystallography (SFX) with X-ray free electron lasers (XFELs) is an emerging field for structural biology. One of its major impacts lies in the ability to reveal the structure of complex proteins previously inaccessible with synchrotron-based crystallography techniques and allowing time-resolved studies from femtoseconds to seconds. The nature of this serial technique requires new approaches for crystallization, data analysis, and sample delivery. With continued advancements in microfabrication techniques, various developments have been reported in the past decade for innovative and efficient microfluidic sample delivery for crystallography experiments using XFELs. This article summarizes the recent developments in microfluidic sample delivery with liquid injection and fixed-target approaches, which allow exciting new research with XFELs.

Keywords Protein · Nozzle · Injector · Fixed-target · Mixing · Time-resolved

Introduction

X-ray crystallography has enabled the determination of high-resolution protein structures that are essential in predicting a protein's function. With the development of serial femtosecond crystallography (SFX) with an X-ray free electron laser (XFEL), crystallographers now have a powerful tool to study proteins and reactions, overcoming limitations of traditional crystallography [1–3]. Due to the ultrafast, highly brilliant X-ray pulses, a protein crystal exposed to a short XFEL pulse can yield a diffraction pattern before the onset of destructive radiation damage, a process termed "diffraction before destruction" [4]. However, since the crystal experiences extensive damage or destruction after a single X-ray exposure, new crystals must be introduced into the path of the XFEL in order to construct a complete electron density map of the protein's structure [2]. Several thousands of diffraction patterns, each pattern obtained from one crystal, are typically needed to obtain a full data set that enables the determination of electron density for a protein structure. Powerful data analysis techniques have been developed in the past years for this purpose, [5–7] to cope with the requirement of SFX with XFELs. This new field has opened the door to studying proteins that do not readily crystallize into large crystals but can crystallize as micro- and nanocrystals [4]. There is even the potential to forgo crystallization altogether and study single particles in solution such as large viruses [8, 9] . Another benefit is that SFX can be performed at ambient temperature and pressure which can more closely model physiological conditions [10]. Furthermore, the short exposure time coupled with the serial introduction of crystals makes SFX a prime target for time-resolved (TR-) studies that elucidate previously unresolved reaction intermediates with the ultimate goal of putting together a "molecular movie" that tracks a reaction as it progresses in time [11].

Currently, there are five operational hard XFEL beamlines: Spring 8-Angstrom Compact free electron Laser (SACLA), Linac Coherent Light Source (LCLS), Pohang Accelerator Laboratory XFEL (PAL-XFEL), European XFEL (EuXFEL), and SwissFEL. The femtosecond X-ray pulse structure varies between beamlines: SACLA, PAL-XFEL, and SwissFEL operate at a maximum of 100 Hz, LCLS operates at up to 120 Hz, and EuXFEL has a 10-Hz bunch train structure, with a projected maximum 4.5-MHz frequency within each 0.6-ms bunch [14, 15]. The current pulse structure at the EuXFEL has a 1.1-MHz frequency with < 1 μs spacing between pulses [16] with about 300 pulses per bunch (which is constantly being improved to meet the final specs of the instrument). As each pulse will destroy the irradiated crystal,

✉ Alexandra Ros
alexandra.ros@asu.edu

[1] School of Molecular Sciences, Arizona State University, Box 871604, Tempe, AZ 85287-1604, USA

[2] Center for Applied Structural Discovery, The Biodesign Institute, Arizona State University, Box 875001, Tempe, AZ 85287-7401, USA

new crystals must be delivered at or exceeding the frequency of the XFEL pulses, which makes the traditional setup of a single looped crystal mounted on a goniometer impractical. To this end, many sample delivery methods have been developed [17], with two main categories: liquid injection or fixed-target approaches, as schematically depicted in Fig. 1. Essentially, all approaches qualify as microfluidic techniques as the critical dimensions of sample delivery are adapted to the size of the crystals used in SFX with XFEL experiments, which ranges from a few micrometers to a few tens of micrometers for most reported experiments. Additionally, since many protein crystals are injected into the path of the XFEL, there is a significant effort to optimize sample delivery methods to reduce sample waste and reduce the time required to collect sufficient data to fully characterize a protein structure. Here, we describe the advancements in sample delivery technology and how they have been applied for SFX and TR-SFX.

Liquid injection devices

Gas dynamic virtual nozzle

Due to the high-intensity X-ray pulses, microcrystals are largely damaged or destroyed when exposed to the X-ray, and a new crystal must be delivered into the X-ray beam by the next pulse. One way to accomplish this high crystal replenish rate is to inject a continuous stream of protein crystal suspension into the X-ray (Fig. 1a). Rayleigh jets were first explored [18] but encountered difficulties: high flow rates (mL/min) and small nozzle orifices are required to create stable jets with a small jet diameter to reduce background scattering from the carrier buffer. The result is an easily clogged nozzle. Furthermore, the Rayleigh jets have a high propensity for ice formation in vacuum, and the intense diffraction from the ice crystals can damage the detector [18].

To overcome the drawbacks, a gas dynamic virtual nozzle (GDVN) was developed that utilizes a coaxially flowing gas to accelerate and focus a liquid stream into a liquid jet [19] (Fig. 2a, b). Pressurized water (frequently from high-pressure liquid chromatography (HPLC) pumps) is used to apply a constant flow rate on a piston within a steel sample reservoir such that the loaded crystal suspension on the opposite side of the piston travels into a fused silica capillary that is interfaced to the GDVN [23]. While nitrogen can be used as a focusing gas, helium is frequently used as it has fewer issues with ice formation in vacuum and results in more stable jet formation, and the lower molecular weight results in less background scattering from X-rays [2]. The first GDVNs were developed using commercially available fused silica capillaries [19]. The smaller liquid capillary is aligned in the center of the larger gas capillary. The end of the gas-focusing capillary is flame polished to decrease the diameter of the gas aperture in order to focus the liquid into a thin jet (< 10 μm) [20]. To decrease the background scattering from the gas-focusing capillary, the nozzle tip is polished into a rounded cone shape [20]. These glass GDVNs were utilized for the early serial crystallography experiments at LCLS [1] and continue as one of the most common injection methods of protein crystals in low-viscosity media, both in vacuum and in ambient pressure [24].

Construction of the outer portion of the GDVN with ceramic materials instead of glass has been explored to increase the nozzle's uniformity and durability [25]. Here, the tip of the nozzle is fabricated by micro-injection molding while the inner capillaries for the gas and liquid lines are polished as in the fused silica GDVNs. The minimum flow rate for stable jetting with ceramic nozzles is similar to that of a glass GDVN, and ceramic nozzles have recently been used for the injection of crystallized fibrils into an XFEL [26]. To further simplify assembly, ceramic nozzles manufactured with powder injection molding [27] have been developed for increased reproducibility of the liquid capillary alignment. Despite their successful use in many XFEL experiments, GDVNs are still mostly assembled manually and require skilled technicians for reliable functioning.

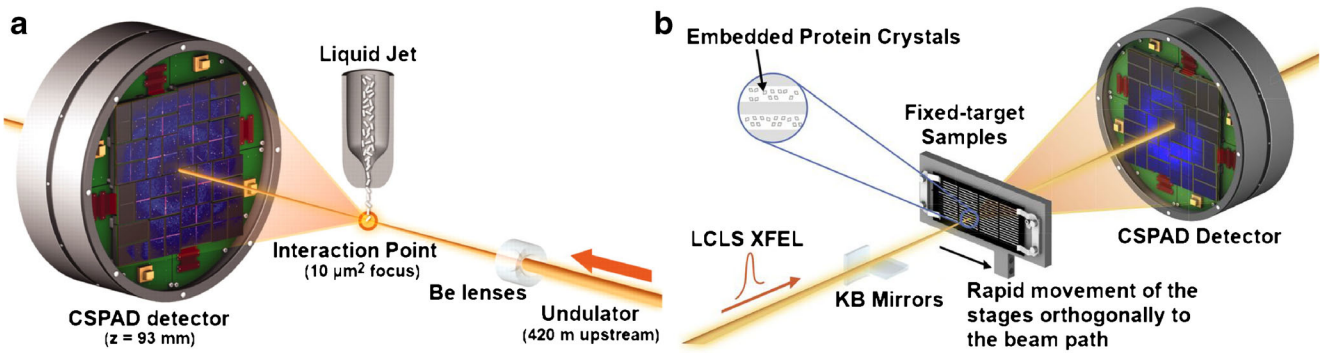

Fig. 1 **a** Overview of an SFX experiment with an XFEL delivering sample with a liquid jet. Reprinted by permission from Boutet et al. [12]. **b** Overview of an SFX experiment with an XFEL employing a fixed-target. Reprinted with permission from Hunter et al. [13]

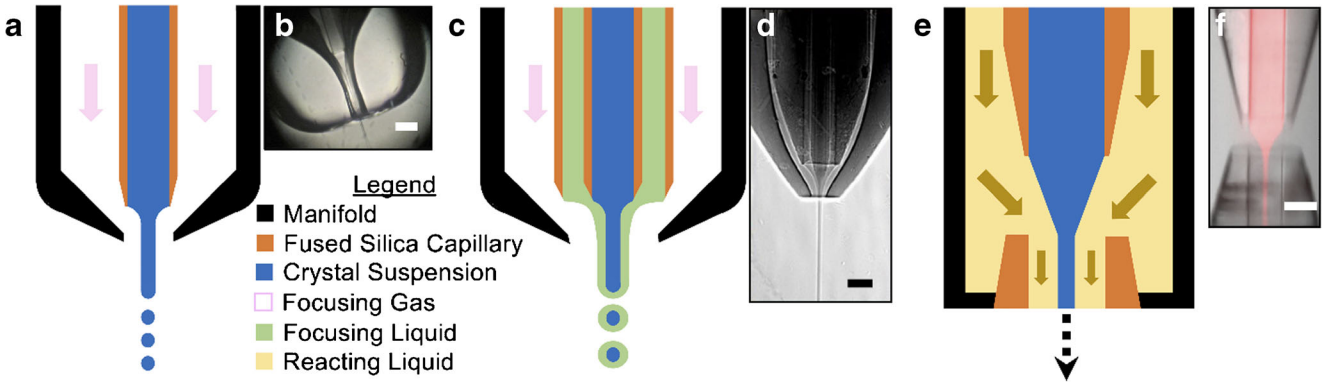

Fig. 2 **a** Schematic and **b** optical microscopy image of a gas dynamic virtual nozzle (GDVN). Adapted and reprinted from Weierstall et al. [20]. **c** Schematic and **d** radiograph of a double flow focusing nozzle (DFFN). Adapted and reprinted with permission from Oberthuer et al. [21]. **e** Schematic and **f** optical microscopy image with an overlaid fluorescence microscopy image of the hydrodynamic focusing region of the mix-and-inject serial crystallography (MISC) injector. Adapted and reprinted from Calvey et al. [22] under a Creative Commons Attribution (CC BY) License. Scale bar for (**b**) and (**d**) is 100 μm, and (**f**) is 50 μm

Microfabricated injectors

In an effort to simplify and automate fabrication, several microfabrication methods for GDVN construction have emerged. For instance, soft lithography was utilized to construct a multilayer polydimethylsiloxane (PDMS) nozzle [28]. The device operates both in vacuum and in ambient pressure, and liquid flow rates are similar to the glass GDVNs, operating between 2 and 8 μL/min, with jet diameters that can extend into the sub-micrometer range. Microfluidics with PDMS has been extensively explored [29, 30], and this fabrication technique has the potential to be coupled to a myriad of microfluidic techniques such as hydrodynamic mixing. However, the elastomer material PDMS may break down or show leaking effects at the high pressures required for GDVN injections at XFEL facilities.

For further fabrication automation, 3D-printed nozzles have been developed [16, 31]. The first custom nozzle designs were realized by computer-aided design (CAD) software in combination with 3D-printing based on the process of two-photon polymerization of a specific resin. Additionally, the nozzles have been utilized at the EuXFEL as the high jet velocities (50–100 m/s) permit sample to be refreshed in the 0.9 μs between pulses within a pulse train (10 Hz) [16]. Even at these velocities, sample consumption can be as low as 13 μL/min depending on nozzle geometry and gas flow rates [16], although between the pulse trains much sample is wasted. Further development was reported by Bohne et al. where 3D-printed nozzles were printed onto a silicon-glass microfluidic device for reduced complexity during assembly, increased repeatability, and interfacing well to the existing on-chip microfluidic applications such as microfluidic mixers and microfilters [32]. This 3D-printing approach eases the layered construction and planar constraints of photolithography; however, the requirements of the printed device geometry require high-resolution 3D-printers, which can currently only be accomplished through two-photon polymerization.

Mix and react injectors

Mixing for time-resolved mix and inject serial crystallography (MISC) is of great interest as the focus of crystallography with XFELs shifts from static structures to dynamic structures of reaction intermediates. MISC experiments have been explored with fused silica GDVNs and an upstream commercial T-junction for mixing and studying reactions on the minute [33] to second time scale [34]. In the former, a ligand binding to a riboswitch RNA is observed with four different structures over the course of the reaction points, including a reaction intermediate, and in the latter studies, the conformational changes that occur when ß-lactamase reacts with the antibiotic ceftriaxone. To reach shorter time points in the millisecond range, MISC injectors with a microfluidic hydrodynamic focusing mixer built into the nozzle have been developed [35]. Here, an inner capillary is aligned coaxially within another liquid capillary. The most central capillary contains the crystal suspension, the outer liquid capillary contains a solution to react with the protein crystals, and a final outermost capillary supplies the focusing gas. More recently, a MISC device with the hydrodynamic focusing mixer at a short distance before the injection nozzle was developed [22] (Fig. 2e, f). The construction of these MISC devices requires access to laser cutting hardware for crafting the device components as well as technical skill for precise manual assembly. Based on the flow rates of the central and focusing liquid as well as the distance from the mixing region to the nozzle aperture, which is tunable during device construction, the reaction time can be adjusted from milliseconds to seconds. This MISC device was utilized at SLAC to mix ß-lactamase with ceftriaxone to study reaction intermediates from 30 ms–2 s [36].

Recently, a MISC method was described that utilized an upstream 3D-printed hydrodynamic mixer coupled to a glass GDVN by a fused silica capillary to study the P_R-intermediate during the catalytic oxidation of cytochrome *c* oxidase [37]. A time point of 8 s was achieved with a long delay line between the mixer and nozzle. The automation of 3D-printing decreases the variability between devices, and a decreased length between the mixer and nozzle will enable reaction time points on the millisecond time scale.

Other approaches

To maintain a stable jet with lower flow rates, a double flow focusing nozzle (DFFN) has been developed that uses a coaxially flowing liquid to accelerate the flow of the inner crystal-containing liquid, both of which are subsequently accelerated by gas focusing to create a jet [21] (Fig. 2c, d). Since the flow rate of the central liquid can be lower than the outer sheath liquid, a thin crystal-containing jet forms within the sheath jet. Due to the reduced volume of the crystal suspension matrix, background scattering can be reduced. Furthermore, the outer sheath liquid has a lower surface tension than the protein crystal suspension; this injection method has increased stability in comparison to injecting the crystal suspension only. Perhaps the greatest benefit of this injection method is the reduced crystal sample flow rate as one of the major drawbacks for GDVNs is the continuous sample injection between X-ray pulses which leads to a majority of the injected sample being wasted. The central sample stream of the DFFN can operate at ~ 5 μL/min, effectively reducing the sample waste by about half.

Pulsed injection

Segment flow droplet injection

The five currently active hard XFEL beamlines—SLAC, SACLA, PAL-XFEL, SwissFEL, and EuXFEL—utilize a pulsed structure to deliver X-rays. As mentioned above, for continuously flowing sample from GDVNs, there is considerable sample waste between X-ray pulses. Depending on the pulse structure of the beamline and the flow rate of the liquid, this can result in > 99% of protein crystals being unseen by the X-rays and therefore not provide diffraction information. Indeed, it has been estimated that 1 out of 10,000 crystals injected using a traditional GDVN results in a diffraction pattern [42]. Given the complexity of protein purification and crystallization, this leads to one of the most severe limitations of SFX with XFELs and has therefore been addressed by several groups. Thus, a way to pulse the injection method such that a sample is present during an X-ray pulse and absent when the laser is "off" is highly desirable.

One method of pulsed injection utilizes a microfluidic droplet generator upstream of the GDVN to segment the aqueous crystal suspension with an oil carrier phase [43]. By varying the liquid flow rates, the frequency of the generated water-in-oil style droplets can be controlled to match the frequency of the XFEL to reduce the amount of sample between droplets (Fig. 3a). The main challenge moving forward will be synchronizing the phase of the droplets with that of the X-ray pulses or pulse trains. To this aim, a 3D-printed droplet generator with built-in electrodes has been developed [38], see Fig. 3b. This device allows droplet generation which can be electrically triggered in a drop-on-demand mode (one trigger pulse yields one droplet generated), a phase shift mode (to shift the phase of the droplet generation while maintaining the frequency), or an acceleration mode (to increase the frequency of the droplet generation). The first and second modes can be used to synchronize sample droplets with the phase of the XFEL pulses to further optimize sample introduction.

Piezoelectric droplet ejection

Instead of continuously injected segmented flow, approaches including piezoelectric elements have demonstrated drop-on-demand ejection into the X-ray beam [39]. The crystal suspension is pressure driven such that a meniscus of the sample is primed to be ejected when agitated by the piezoelectric element that is triggered by an electric pulse generator at the frequency and phase of the XFEL (Fig. 3c, d). This has been demonstrated with a repetition rate of 30 Hz and a crystal suspension of lysozyme crystals in a helium environment [39]. Considerable savings in sample amount (1–2 orders of magnitude) can be accomplished using this droplet injection method and it has been applied for crystallographic studies on lysozyme [39] and bacteriorhodopsin [44]. The droplet diameter of ~ 80 μm is large in comparison to typical GDVN jet diameters (< 10 μm), which can result in higher background scattering, and this method may have difficulties with ice formation in vacuum. However, a study comparing the piezoelectrically pulsed droplet injection to GDVN injection found that there was no significant difference in the limiting diffraction resolution when studying a photochromic fluorescent protein [24].

Acoustic droplet ejection (ADE)

Similar to the previous method, crystal suspension in ambient pressure conditions can be acoustically ejected as a droplet from a well plate into the path of the X-ray [40] (Fig. 3e, f). The acoustic pulse is synchronized to the X-ray frequency, resulting in a high droplet hit rate (here defined as the number of droplets hit divided by the total number of X-ray pulses) of up to 88% and up to two orders of magnitude less volume of protein crystal suspension required to solve a complete

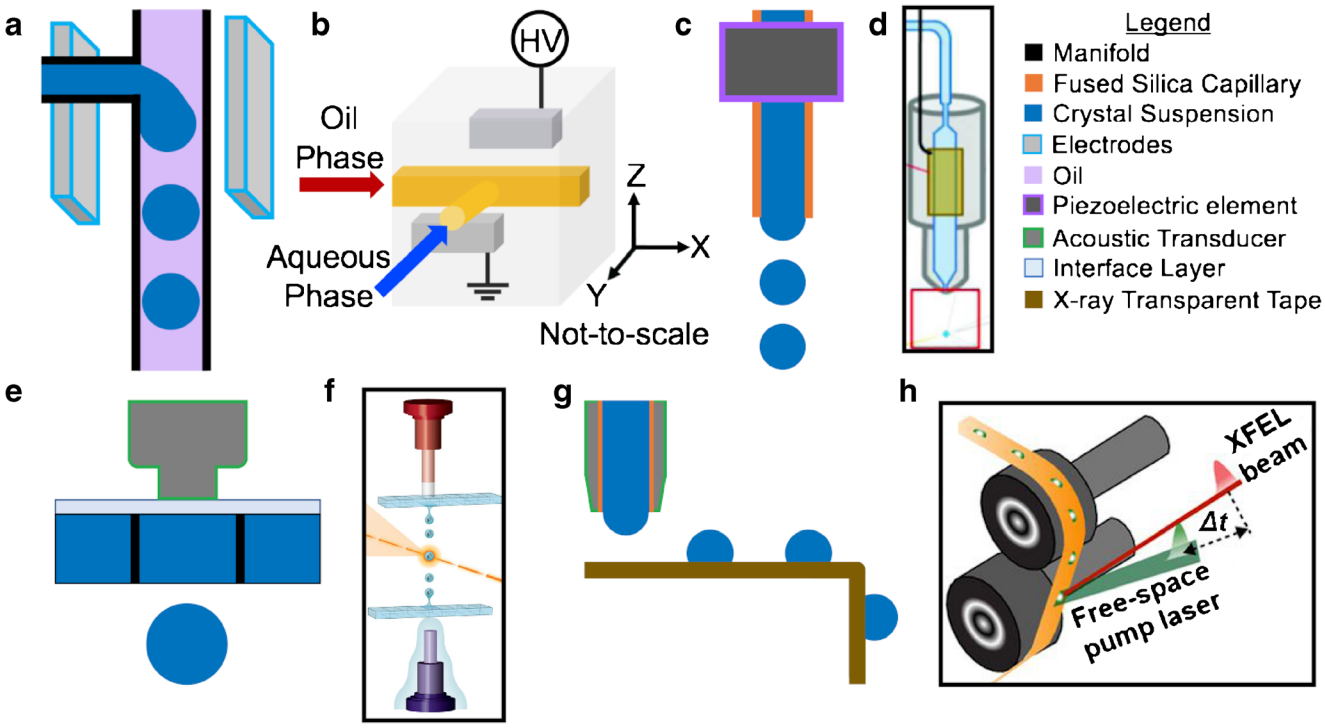

Fig. 3 **a** Schematic of droplet generation and **b** 3D layout of the geometry for the electrically triggered microfluidic droplet generator. Adapted from Kim et al. [38]. **c**, **d** Schematics of the piezoelectrically actuated droplet injector. Adapted and reproduced from Mafune et al. [39] with permission of the International Union of Crystallography. **e** Schematics of an acoustic droplet ejection (ADE) injector. **f** Schematic illustrating ADE injection from below and above the sample well. Adapted and reprinted from Roessler et al. [40]. **g**, **h** Schematics of ADE combined with droplets on tape (DOT) for sample delivery. Adapted and reprinted by permission from Fuller et al. [41]

electron density structure. The main benefit is the reduction in protein crystal consumption: on average, for every two crystals injected, one diffraction pattern is recorded which corresponds to a crystal hit ratio up to 50% (defined as the number of images containing Bragg peaks from crystals per droplet probed). In ADE, the crystal hit ratio is still determined by the crystal density, although the concentration can be increased by allowing the crystals to settle in the meniscus of a droplet and ejecting the droplets downward. However, if the crystal density is too high, clogging can occur caused by insufficient acoustic forces to eject a droplet, therefore care must be taken to balance high crystal hit ratios with effective droplet ejection. Additionally, by adjusting the acoustic frequency, the droplet size can be tuned, and this method works for crystal suspensions in a range of buffer compositions and viscosities [40]. While ADE works for crystals as small as 5 μm, it is optimized for larger crystals (>50 μm) as the ejected droplet has a large diameter (~60–170 μm) that yields higher background scattering than the thin jets of a GDVN.

Droplet on tape

An X-ray transparent conveyor belt can be coupled with ADE to make a DOT method of delivering crystals to the XFEL [41]. The droplets are deposited onto the conveyor belt tape on which they are transported into the path of the X-ray (Fig. 3g). Droplet synchronization with the XFEL and any upstream time-resolved excitation periphery is accomplished with a complex combination of the conveyor belt tape speed, the ADE trigger (attained from the XFEL master clock), and micromanipulation of upstream optical fibers aided by inline cameras (Supplemental Information of Fuller, F. D. et al. [41]). Indeed, the setup of the DOT method is non-trivial and required three experts to devote 5 days toward DOT assembly and optimization (Supplemental Information of Fuller, F. D. et al. [41]). The X-ray beam itself is parallel to the tape, thereby intersecting the crystal-containing droplet without damaging the tape (Fig. 3h). After a cleaning step, the tape is recycled allowing this method to work continuously for long periods of time. With an X-ray frequency of 10 Hz, DOT has demonstrated up to 100% droplet hit rate [41], with the crystal hit ratio still dependent on crystal concentration in the droplet. Droplet delivery of up to 60 Hz has been demonstrated for X-ray emission spectroscopy (XES) at an XFEL [41] and can extend up to 120 Hz. On the way to the beam, the droplets can be photoactivated by a series of optical pump probe lasers, and based on the tape velocity, a TR-SFX experiment can be performed. For example, the structural changes for the various intermediate states of photosystem II (PSII) after photoexcitation were observed [46]. Instead of a pump probe setup, a gas chamber can be installed for chemically triggered reactions such as oxygen reacting with

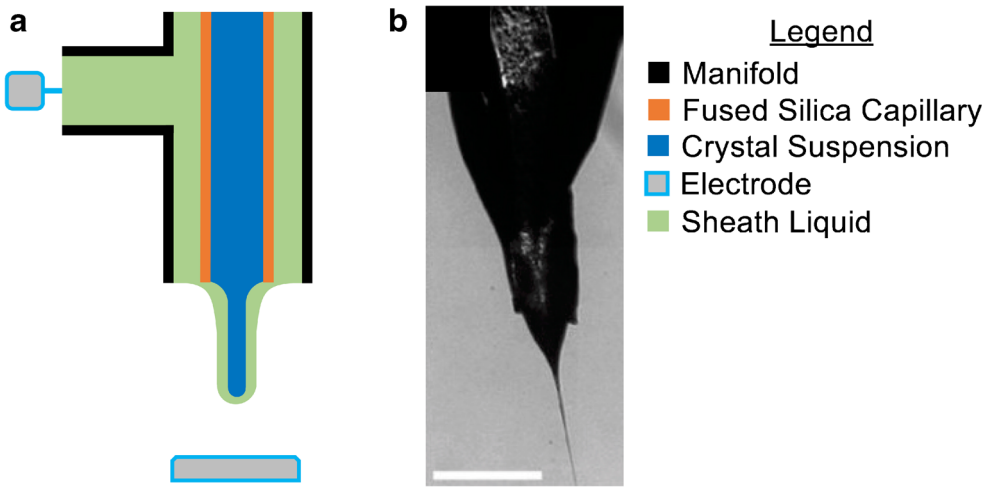

Fig. 4 **a** Schematic of the CoMESH injector and **b** an optical microscopy image of injected PSII crystals. Adapted and reprinted by permission from Sierra et al. [45]. Scale bar is 360 μm

ribonucleotide reductase R2. The reaction time points capable of being probed with this method range from hundreds of milliseconds to seconds [41]; however, the time resolution may not be suitable for fast reactions and is currently limited to gaseous reactants.

Electrospinning

Microfuidic electrokinetic sample holder

By applying a potential between a liquid and an electrode, a liquid stream can become a liquid jet in a process called electrospinning [47]. The neck of the jet is similar to the jet produced by the GDVN and can be used as a continuous injection method for SFX [48]. The microfluidic electrokinetic sample holder (MESH) injector [48] is gentle on the crystals as there is no traditional Rayleigh nozzle, and the capillary delivering the crystals can be larger than those found in a GDVN which sidesteps the need for crystal filtering. The original design for the MESH injector required the crystal suspension to include glycerol in order to extend the neck of the jet and decrease the likelihood of dehydration and freezing after the liquid has exited the orifice. While a benefit is that glycerol would decrease the speed at which crystals settled in a reservoir, the drawback is that not all crystals remain stable when mixed with glycerol.

Concentric MESH

In order to solve this problem, a concentric MESH (CoMESH) injector was developed [45]. Operating off the same principle as the MESH injector, the CoMESH has a capillary containing a sheath liquid that concentrically surrounds the capillary containing the crystal suspension (Fig. 4). This sheath liquid contains components such as 2-methyl-2,4-pentanediol to prevent dehydration and freezing due to the vacuum environment. In this way, the crystals can stay in the preferred mother liquor while a jet is maintained due to the stability of the sheath liquid. Additionally, since the sheath liquid only comes in contact with the crystal suspension immediately before jetting, not enough time is present for the sheath liquid to destabilize the crystals. A potential of up to 5000 V is applied to generate a jet, and the flow rates required for jetting (0.8–3.0 μL/min) are about an order of magnitude smaller than jetting with a GDVN.

The CoMESH has been used to study both static structures and time-resolved structures at XFEL facilities. The structure of a bacterial 30S ribosomal subunit was determined with SFX with electrospinning injection and subsequently compared to the structure obtained by cryo-crystallography [49, 50]. In the same study [50], the structures of several aminoglycosides bound to the ribosome were determined, and the effect of temperature on the protein structures was revealed. For photoactivated TR-SFX with MESH injection, the Mn_4CaO_5 cluster in PSII was studied by simultaneous X-ray diffraction with an XFEL and XES with an optical laser [51]. Photoactivated TR-SFX of PSII injected by electrospinning (this time using the CoMESH) was later revisited to further study the production of oxygen [46]. High-resolution structures for the dark state and one of the photoexcited states were obtained.

Viscous media injection

Lipidic cubic phase

For a typical GDVN, the vast majority of the injected sample volume is unseen by the X-ray and is wasted [42]. Therefore, another route for reducing sample consumption is to decrease the flow rate of the jet, and consequently the jet velocity, so that less sample is injected between pulses. To reduce the liquid flow rate below what has been demonstrated with a

DFFN and electrospinning, high-viscosity crystal-containing media that maintain a jet-like extrusion even at sub-μL/min flow rates have been explored. One of the most widely applied high-viscosity crystal media is lipidic cubic phase (LCP), which is especially useful for membrane proteins: LCP can mimic the lipid bilayer in which the proteins are natively embedded, and some proteins can also be crystallized in LCP and remain in their natural crystallization environment during X-ray diffraction as successfully demonstrated by Cherezov and coworkers for various membrane proteins [52, 53]. Furthermore, the crystals grown in LCP are typically microcrystals that are well suited for SFX with XFELs, and the high viscosity prevents crystal settling in the reservoir, avoiding the need for an anti-settling device. One of the most noteworthy successes of SFX using LCP has been the structure determination of G protein-coupled receptors (GPCRs), proteins that are vital for regulating many biological processes in humans, which were challenging to study with third-generation synchrotron sources due to their dynamic nature that leads to complex crystallization and stabilization conditions [54, 55]. Of particular note, SFX with LCP has been used to obtain higher resolution structures than previous synchrotron diffraction experiments, and novel GPCR structures have been solved with de novo phasing methods [54, 55]. It should be noted that the composition of the LCP is crucial as the transition to any other phase, such as to the lamellar phase must be avoided to protect the detector from too strong diffraction [42]. In addition, the high viscosity of the LCP will typically rapidly clog the GDVN and thus requires specialized injectors.

To overcome this limitation, Weierstall et al. [42] developed an injector which extrudes the viscous LCP at a pressure between 2000 and 10,000 psi, therefore requiring a modification to the sample reservoir. Water pressurized through an HPLC pump exerts a force on a large steel plunger that is connected by a narrow rod to two Teflon balls present before the LCP in the reservoir (Fig. 5). In this way, the applied pressure is amplified by a factor of 34, so lower upstream pressures can be utilized to extrude the LCP. The sample reservoir is built into the LCP injector and is located immediately before the nozzle. The extruded LCP is stabilized by a focusing gas, typically nitrogen or helium, and the flow rate of the LCP is chosen to match the frequency of the XFEL so that new sample is refreshed between X-ray pulses and excess sample injected is minimized. Ultimately, LCP injection can result in up to two orders of magnitude less protein used than with typical GDVN injection to acquire the same amount of data. A drawback of using this method is the large jet diameter (~ 50 μm) in comparison to the GDVN (< 10 μm) which increases the background scattering and complicates data analysis.

Alternative high viscosity media

As not all proteins grow into crystals in LCP, other viscous media have been explored. By mixing crystals in their mother liquor with a grease matrix, the crystals stay within media sustaining their integrity while being suspended in the highly viscous grease. The grease mixture can be extruded from a narrow-bore tip (e.g., 110-μm inner diameter) into the XFEL at flow rates as low as 120 nL/min for a 30-Hz X-ray frequency [56]. Using this same method of mixing and extrusion, hyaluronic acid has been used as a water-based viscous medium for protein crystals that are grease-sensitive [57]. Additionally, hyaluronic acid has demonstrated weaker background scattering in comparison to grease methods.

Other media, such as agarose, can also be used with the LCP injector [58]. While grease methods have only been demonstrated in ambient pressure, agarose can be employed as a medium for crystals that are not compatible with LCP and, when mixed with a cryoprotectant like glycerol, can be used to extrude a high viscosity jet at low flow rates in vacuum. An additional benefit is the reduced background scattering with agarose in comparison to LCP or a grease matrix; working in vacuo further reduces background. Conrad et al. obtained a structure of phycocyanin at 2.5 Å with agarose as the viscous medium combined with an LCP injector. [58]

Recently, polyacrylamide has been studied for use as a high-viscosity carrier matrix for protein crystals [59]. When compared to the monoolein in LCP, polyacrylamide shows

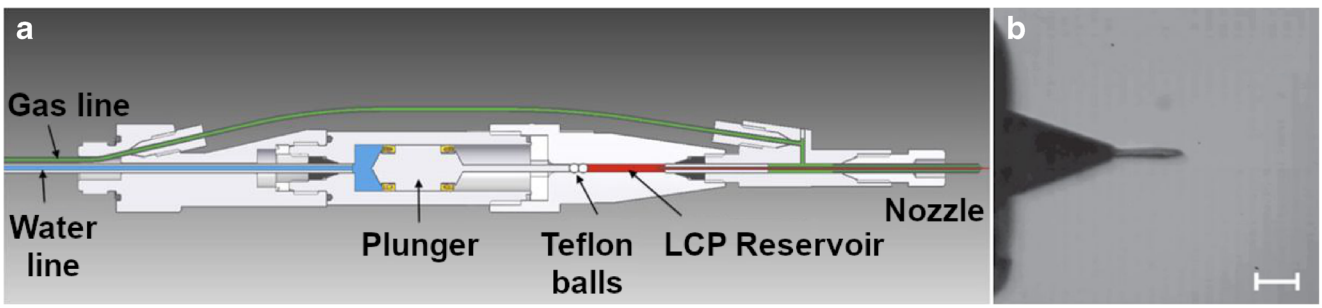

Fig. 5 **a** Schematic of the LCP injector and **b** optical microscopy image of a jet of 9.9 MAG LCP in vacuum. Both **a** and **b** are adapted and reprinted by permission from Weierstall et al. [42]. Scale bar is 100 μm

less maximum background scattering. Both lysozyme and thermolysin crystals were injected using a carrier matrix delivery injector (similar to the LCP injector) at PAL-XFEL, and structures were solved to 1.7 Å and 1.8 Å, respectively [59].

TR-SFX applications for viscous media

The LCP injector has been successfully employed for TR-SFX, with photoactivated proteins as a prime target. The protein crystals extruded in the LCP jet are irradiated by an optical laser just before being intersected by the X-ray beam. For instance, bacteriorhodopsin (bR) can act as a proton pump when triggered by light and has been a key target for TR-SFX in LCP [60, 61]. The time delay between the optical laser pump probe and the X-ray determines the intermediate species of the protein. The time delays can be from the millisecond [60] over nanosecond [61] down to picosecond time range [62], although the sample flow rate must be increased above 5 μL/min for the shorter time delays. The ultimate goal of such time-resolved studies is a "molecular movie," that allows researchers to follow the structural changes upon light excitation.

Similar to LCP, grease has been used for TR-SFX studies at SACLA. Structural changes for PSII on the millisecond time scale were observed out to 2.35 Å using a grease jet extruded from a syringe [63]. Another avenue for pump probe style TR-SFX is using photocaged compounds. Photocaged nitric oxide (NO) was injected in a hydroxyethyl cellulose matrix by an LCP injector, and upon irradiation with UV light, it was released to react with the P450, a protein that catalyzes NO to nitrous oxide, for 20 ms before X-ray exposure [64]. From this, an ambient temperature 2.1 Å structure of the P450nor intermediate was determined.

Aerosol injection

Aerodynamic Lens stack

As a result of the ultrashort pulses and high brightness of XFELs, another frontier is the ability to obtain diffraction from large single particles, for instance, viruses [8, 65]. A benefit of using non-crystalline samples is that protein samples do not need to be crystallized which eliminates much of the sample preparation required in crystallography with the previously mentioned methods. However, since single particles have very weak diffraction intensity in comparison to crystals, background from a liquid jet would dwarf any signal obtained from the analyte [66]. As such, aerosolized samples are a promising method of sample introduction for non-crystalline samples at XFELs. An aerodynamic lens stack that focuses an aerosol into a thin particle beam has been developed and employed to obtain diffraction at a synchrotron [9]. The diameter of these particle beams can range from hundreds to tens of micrometers. The aerodynamic lens stack was utilized at the atomic, molecular and optics (AMO) end station at LCLS to study carboxysomes [67, 68]. Hit rates (here defined as the number of images containing Bragg peaks per total number of X-ray pulses) were about 79%, and the sample volume used was only 36 μL.

Convergent nozzle aerosol injector

In an effort to minimize both the setup and the diameter of the focused aerosol, a single orifice convergent nozzle aerosol injector (CNAI) was developed [69]. In this case, a GDVN upstream of the convergent nozzle generates an aerosol at ambient pressures, and the geometry of the nozzle accelerates the aerosol particles along convergent gas streamlines as they transverse the orifice into the vacuum chamber. The result is an aerosol with a sub-ten-micrometer diameter focal point that is several hundred micrometers from the nozzle orifice. This CNAI was utilized at the coherent X-ray imaging (CXI) beamline at LCLS to image granulovirus ($200 \times 200 \times 370\ nm^3$) surrounded by a crystalline shell [70]. In comparison to liquid jets such as the GDVN, one would expect a decreased hit rate since the particles injected by the CNAI have a velocity ~25× greater and have a reduced liquid flow rate. The predicted particle hit rate for the CNAI was 0.04–0.4%; however, the experimental particle hit rate was substantially lower at 0.006%. Currently, the very low hit rate is a bottleneck for single particle imaging work at XFELs with CNAIs.

Aerosolization by desorption

An innovative method that combines fixed-target with aerosolized injection is desorption by impulsive vibrational excitation (DIVE) with a picosecond IR laser (PIRL) [71]. In this method, crystal sample in solution deposited on a substrate is irradiated by a PIRL and the contents are ejected in a plume upwards into the path of the X-ray. The PIRL is relatively gentle on the crystals, with the crystal diffraction quality essentially unaffected by this injection method. The authors also mention that the sample does not need to have crystals, opening the door for single-particle diffraction if the aerosol has sufficiently low background signal intensity to differentiate the analyte signal.

Sample delivery for fixed-target experiments

While liquid delivery at XFEL experiments has been the method of choice in the early years, delivery of crystals on a solid support or so-called fixed-target has also been explored recently. Typically, fixed-target crystallographic experiments

refer to the case where crystals are loaded on a solid matrix in the path of an X-ray source to obtain the diffraction data, as shown in Fig. 1b [4, 72]. These matrices are often microfabricated and micropatterned chips that allow fast and reproducible loading of thousands of crystals in a reproducible manner. This highly efficient method of crystal delivery not only significantly decreases the amount of required sample in comparison with liquid injection methods discussed above (typically a few μL) but can also be readily modified for crystals ranging from sub-micrometer to 100 μm in size. These chips can also be developed to support room and cryo temperature conditions. Furthermore, such microfabricated devices offer spatial control over crystal location and orientation on-chip, and they can be exploited for high-throughput automated serial crystallographic applications using high-speed translation stages at various XFEL and synchrotron beamlines [72, 73]. In the case of XFELs, fixed-target applications offer further potential as high energy femtosecond X-ray pulses can be used to gather diffraction data prior to onset of radiation damage on the crystal [1, 4]. Other than holding crystals, microfluidic devices have also gained immense interest recently for integrated on-chip crystallization and fixed-target applications, eliminating the cumbersome and error-prone process of harvesting crystals from conventional crystallization methods prior to X-ray diffraction. Recently, a number of such microfluidic fixed-target devices have surfaced for both on-chip crystallization and diffraction studies at XFEL sources and are discussed below.

Silicon micropatterned chips

Silicon-based micropatterned chips and trap arrays, offering low background scattering, have been widely exploited for fixed-target X-ray diffraction studies. Hunter et al. [13] reported an etched silicon nitride membrane chip as a fixed-target solid support for microcrystals of rapid encystment protein (24 kDa, REP24) embedded in Paratone-N for crystallographic studies at LCLS. The device was used to perform SFX at a high resolution of ~2.5 Å with an acquisition rate of 10 Hz and a hit rate of ~38% (Fig. 1b). Murray et al. [74] also reported a three-layer microdiffraction device made from silicon nitride, photoresist and polyimide film for studying Hen egg-white lysozyme (HEWL) microcrystals, as shown in Fig. 6a. HEWL microcrystals (~10–15 μm in size) were used for room temperature X-ray diffraction experiments at the LCLS X-ray Pump Probe (XPP) end station and other synchrotron beamlines. Diffraction experiments were performed using a 3–30 μm unattenuated beam with 40-fs pulses, and microcrystal images were taken manually by focusing on the silicon nitride window present on the chip. Using this chip, a high-resolution (~1.5 Å) diffraction data set was reported from 324 diffraction images.

Mueller et al. [75] reported another silicon-based crystal holder chip as a fixed-target matrix for room temperature serial crystallographic applications at XFEL and synchrotron sources. The crystal holder chip was microfabricated from a silicon wafer using photolithographic, plasma etching, and wet etching

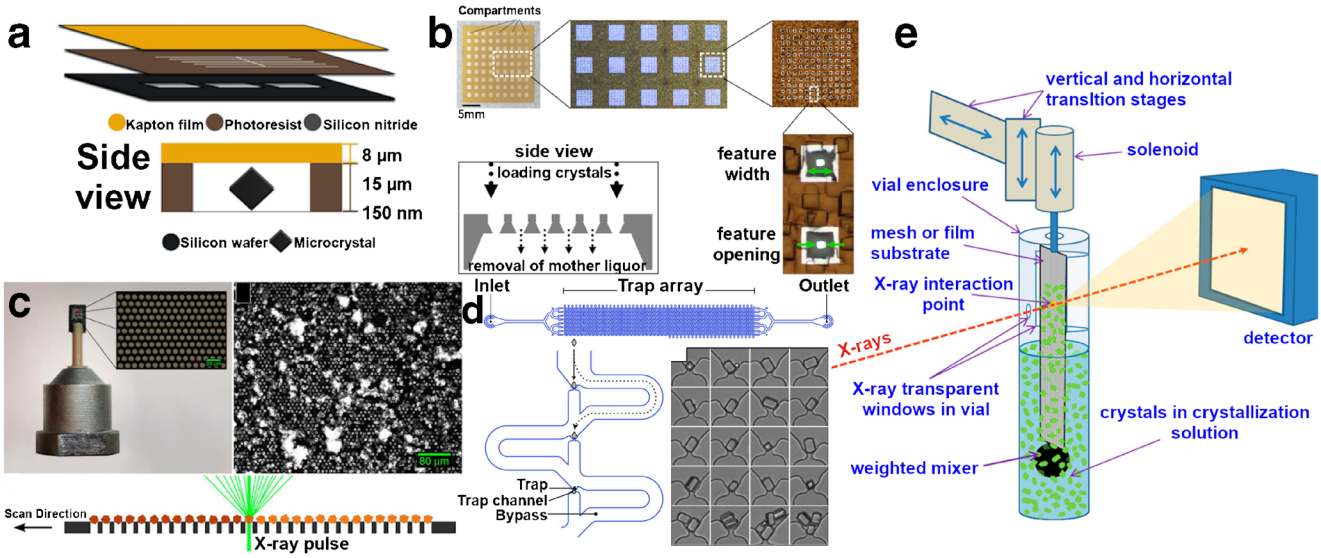

Fig. 6 Sample delivery for fixed-target diffraction experiments. **a** A schematic of the three-layer microchip crystal holder device fabricated from a silicon wafer, photoresist, and Kapton. Adapted and reprinted with permission from Murray et al. [74]. **b** A Silicon chip with an array of tapered holes for holding crystals to conduct time-resolved crystallographic experiments. Reprinted from Mueller et al. [75] under a CC BY License. **c** A silicon chip with micropores for holding crystals (right) mounted on a "Roadrunner" Goniometer (left) along with crystal scanning strategy for high-speed fixed-target viral crystallography (bottom). Adapted and reprinted with permission from Roedig et al. [76]. **d** A schematic of a PDMS-PMMA microfluidic device with Trap-and-Bypass array for crystal capture with a micrograph of trapped HEWL microcrystals. Adapted and reprinted with permission from Lyubimov et al. [77]. **e** An overview of a fixed-target serial crystallography experiment using a nylon mesh-based crystal extractor positioned through translation stages. Reprinted with permission from Mathews et al. [78]

techniques to create a matrix of tapered through holes to filter crystals of 30–60-μm size from their mother liquor prior to fixed-target experiments, as shown in Fig. 6b. Using this device, crystals of sperm whale myoglobin bound with carbon monoxide (SWMb-CO) were used to conduct time-resolved crystallographic experiments at LCLS. Recently, the same group reported additional improvements to the first-generation chip by combining spectroscopic mapping of crystals prior to X-ray diffraction to achieve an overall hit rate up to 85%, further decreasing the required sample volume [79]. Using this device, SWMb-CO crystals were used to obtain an X-ray diffraction data set with a resolution of ~ 1.3 Å at the XPP end station. Nam et al. [80] reported a silicon nitride membrane-based fixed-target diffraction chip for single-shot imaging of biological and non-biological specimen. The chip was composed of an array of 200 μm × 200 μm windows of 100-nm-thick negatively charged silicon nitride membrane, and monodisperse metallic nanoparticles were either air dried or spin coated on the chip. Employing the same device, RNAi microsponges could be sandwiched between two silicon nitride membranes. These fixed-target diffraction experiments were conducted at SACLA with a 1.5-μm focused beam (10-fs pulses) at 30 Hz.

Recently, Roedig et al. [76] reported a micropatterned silicon chip mounted on a high-speed goniometer—termed the "Roadrunner"—for serial X-ray crystallography at XPP end station. As shown in Fig. 6c, the silicon chip contained a grid of micropores (size 4–8 μm) to accommodate crystals of picornavirus bovine enterovirus 2 (BEV2) and cytoplasmic polyhedrosis virus type 18 polyhedrin (CPV18). The chip was mounted on the Roadrunner goniometer for high-speed raster scanning at a repetition rate of 120 Hz. Using this high-speed setup, a maximum hit rate of ~ 10 and ~ 70% and resolution of 2.3 Å and 2.4 Å was reported for BEV2 and CPV18 crystals, respectively.

Alternative materials for micropatterned fixed-target chips

Due to the nature of fixed-target X-ray diffraction experiments, there is constant need for microfabrication materials exhibiting high X-ray permeability and low background scattering. Thus, numerous new device fabrication materials (other than micropatterned silicon chips) like PDMS, poly (methyl methacrylate) (PMMA), and cyclic olefin copolymer (COC) have also been explored. Lyubimov et al. [77] reported a microfluidic trap array chip fabricated from PDMS on a PMMA substrate for trapping microcrystals for X-ray diffraction studies. Two types of crystal trapping array designs were explored (weir-type and trap-and-bypass designs). After initial testing, the trap-and-bypass design was chosen for crystal trapping due to its comparatively high trapping efficiency, shown in Fig. 6d. Using this microcrystal trapping device, HEWL microcrystals were trapped and used for room temperature X-ray diffraction studies at XPP and synchrotron beamlines with resolutions up to 1.8 Å. Mathew et al. [78] recently reported a nylon mesh-based crystal extractor for serial crystallography experiments also at XPP end station. The nylon mesh extractor contained diamond-shaped holes and was dipped in solution of trans-acyltransferase crystals to extract the crystals prior to X-ray exposure using translation stages, as shown in Fig. 6e. Out of ~ 23,000 images collected in ~ 40 min, about 2000 images contained sufficient diffraction information (a hit rate of ~ 10%) to obtain a full data set with a resolution of 2.5 Å. Very recently, Górzny et al. [81] proposed a hybrid microfluidic device capable of forming on-chip lipid bilayers to perform fixed-target experiments on membrane proteins in their native state using XFELs. The device integrated etched silicon nitride windows sandwiched between two channels formed by PDMS layers for introducing electrolyte solution and lipids resulting in the formation of a lipid bilayer at silicon nitride windows. The presence of the lipid bilayer was verified using impedance spectroscopy as the measured impedance increased from kΩ to GΩ for empty chip and chip containing lipid bilayer, respectively. Such a conceptual microfluidic device may offer great potential for diffraction experiments on membrane proteins in the future. Additionally, a number of hybrid COC-PDMS devices have been recently reported by several research groups for fixed-target X-ray diffraction experiments at Synchrotron beamlines that may also be modified for XFEL-based diffraction experiments [17, 72, 82, 83].

Chip-less fixed-target

Despite low sample requirements for the aforementioned fixed-target chips, microfabrication of such platforms and crystal loading may still pose some challenges. Thus, some researchers are working on thin film adaptation of fixed-target chips. Very recently, Doak et al. [84] reported a "chip-less" approach for fixed-target crystallization experiments using crystal solution sandwiched between two Mylar sheets (2.5-μm thickness). Microcrystals of carboxyhemoglobin and lysozyme were used for SFX data collection at SACLA using this sheet-on-sheet setup with a hit rate of 10–30% and resolutions down to ~ 2.1 Å. Such "sheet-on-sheet" platforms may require larger sample volumes as compared to micropatterned chips but are comparatively inexpensive and may eliminate cumbersome microfabrication processes requiring a cleanroom facility as well as challenges with on-chip crystal loading.

Conclusion and outlook

Due to the many variations in beamline parameters, crystal stability, and experimental design, there has yet to be a catch-all sample delivery method for the exciting field of SFX and TR-SFX with XFELs. Optimization continues for methods such as the GDVN and viscous media injectors that

see widespread use and have shown to support exciting new insight into protein structure. Previously inaccessible crystal samples are also being explored with methods such as electrospinning and ADE, and efforts are being conducted in the community to even explore TR-mixing experiments with viscous LCP injectors. With the increased resolution of 3D printers, microfluidics coupled to various injection methods is a rapidly developing frontier. This may eventually allow integration of various functionalities, such as mixers, injectors, and droplet generators, to name a few and greatly facilitate sample delivery for challenging experiments such as TR studies. Advancements in fixed-target devices, requiring low sample volumes and eliminating the crystal harvesting processes, have also paved the path for high-efficiency X-ray diffraction experiments for proteins that are difficult to crystallize in suitable concentrations and volumes. Furthermore, recently explored novel device fabrication materials offering low background scattering and high X-ray transparency may offer high-resolution diffraction data. Such devices can also offer crystal mapping prior to diffraction experiments ensuring high crystal hit rate which is crucial considering the scarcity of protein crystal samples and beamtime availability. While the lack of access to XFEL facilities remains one of the major bottlenecks, such advancements in sample delivery technology may allow researchers to collect more data with less sample volume in a shorter time in the future.

Acknowledgments Financial support from the STC Program of the National Science Foundation through BioXFEL under Agreement No. 1231306 and the National Institutes of Health Award No. R01GM095583 is gratefully acknowledged.

Compliance with ethical standards

Conflict of interest The authors declare that they have no conflict of interest.

References

1. Chapman HN, Fromme P, Barty A, White TA, Kirian RA, Aquila A, et al. Femtosecond X-ray protein nanocrystallography. Nature. 2011;470(7332):73–7.
2. Schlichting I. Serial femtosecond crystallography: the first five years. IUCrJ. 2015;2(2):246–55.
3. Chapman HN. X-ray free-electron lasers for the structure and dynamics of macromolecules. Annu Rev Biochem. 2019;88(1).
4. Neutze R, Wouts R, van der Spoel D, Weckert E, Hajdu J. Potential for biomolecular imaging with femtosecond X-ray pulses. Nature. 2000;406(6797):752–7.
5. Barty A, Kirian RA, Maia FR, Hantke M, Yoon CH, White TA, et al. Cheetah: software for high-throughput reduction and analysis of serial femtosecond X-ray diffraction data. J Appl Crystallogr. 2014;47(3):1118–31.
6. White TA, Kirian RA, Martin AV, Aquila A, Nass K, Barty A, et al. CrystFEL: a software suite for snapshot serial crystallography. J Appl Crystallogr. 2012;45(2):335–41.
7. White TA. Processing serial crystallography data with CrystFEL: a step-by-step guide. Acta Crystallogr D Struct Biol. 2019;75(2):219–33.
8. Spence JC, Doak RB. Single molecule diffraction. Phys Rev Lett. 2004;92(19):198102.
9. Bogan MJ, Benner WH, Boutet S, Rohner U, Frank M, Barty A, et al. Single particle X-ray diffractive imaging. Nano Lett. 2008;8(1):310–6.
10. Johansson LC, Stauch B, Ishchenko A, Cherezov V. A bright future for serial femtosecond crystallography with XFELs. Trends Biochem Sci. 2017;42(9):749–62.
11. Barty A, Kupper J, Chapman HN. Molecular imaging using X-ray free-electron lasers. Annu Rev Phys Chem. 2013;64(1):415–35.
12. Boutet S, Lomb L, Williams GJ, Barends TR, Aquila A, Doak RB, et al. High-resolution protein structure determination by serial femtosecond crystallography. Science. 2012;337(6092):362–4.
13. Hunter MS, Segelke B, Messerschmidt M, Williams GJ, Zatsepin NA, Barty A, et al. Fixed-target protein serial microcrystallography with an x-ray free electron laser. Sci Rep. 2014;4(1):6026.
14. Lee J-H, Zatsepin NA, Kim KH. Time-resolved serial femtosecond X-ray crystallography. BioDesign. 2018;6(1):15–22.
15. Altarelli M, Mancuso AP. Structural biology at the European X-ray free-electron laser facility. Philos Trans R Soc Lond Ser B Biol Sci. 2014;369(1647):20130311.
16. Wiedorn MO, Oberthur D, Bean R, Schubert R, Werner N, Abbey B, et al. Megahertz serial crystallography. Nat Commun. 2018;9(1):4025.
17. Martiel I, Muller-Werkmeister HM, Cohen AE. Strategies for sample delivery for femtosecond crystallography. Acta Crystallogr D Struct Biol. 2019;75(2):160–77.
18. Weierstall U. Liquid sample delivery techniques for serial femtosecond crystallography. Philos Trans R Soc Lond Ser B Biol Sci. 2014;369(1647):20130337.
19. DePonte DP, Weierstall U, Schmidt K, Warner J, Starodub D, Spence JCH, et al. Gas dynamic virtual nozzle for generation of microscopic droplet streams. J Phys D Appl Phys. 2008;41(19):195505.
20. Weierstall U, Spence JC, Doak RB. Injector for scattering measurements on fully solvated biospecies. Rev Sci Instrum. 2012;83(3):035108.
21. Oberthuer D, Knoška J, Wiedorn MO, Beyerlein KR, Bushnell DA, Kovaleva EG, et al. Double-flow focused liquid injector for efficient serial femtosecond crystallography. Sci Rep. 2017;7(1):44628.
22. Calvey GD, Katz AM, Schaffer CB, Pollack L. Mixing injector enables time-resolved crystallography with high hit rate at X-ray free electron lasers. Struct Dyn. 2016;3(5):054301.
23. Lomb L, Steinbrener J, Bari S, Beisel D, Berndt D, Kieser C, et al. An anti-settling sample delivery instrument for serial femtosecond crystallography. J Appl Crystallogr. 2012;45(4):674–8.
24. Hutchison CDM, Cordon-Preciado V, Morgan RML, Nakane T, Ferreira J, Dorlhiac G, et al. X-ray free electron laser determination of crystal structures of dark and light states of a reversibly photoswitching fluorescent protein at room temperature. Int J Mol Sci. 2017;18(9):1918.
25. Beyerlein KR, Adriano L, Heymann M, Kirian R, Knoska J, Wilde F, et al. Ceramic micro-injection molded nozzles for serial femtosecond crystallography sample delivery. Rev Sci Instrum. 2015;86(12):125104.
26. Wojtas DH, Ayyer K, Liang M, Mossou E, Romoli F, Seuring C, et al. Analysis of XFEL serial diffraction data from individual crystalline fibrils. IUCrJ. 2017;4(6):795–811.
27. Piotter V, Klein A, Plewa K, Beyerlein KR, Chapman HN, Bajt S. Development of a ceramic injection molding process for liquid jet nozzles to be applied for X-ray free-electron lasers. Microsyst Technol. 2018;24(2):1247–52.

28. Trebbin M, Kruger K, DePonte D, Roth SV, Chapman HN, Forster S. Microfluidic liquid jet system with compatibility for atmospheric and high-vacuum conditions. Lab Chip. 2014;14(10):1733–45.
29. Sia SK, Whitesides GM. Microfluidic devices fabricated in poly (dimethylsiloxane) for biological studies. Electrophoresis. 2003;24(21):3563–76.
30. Nguyen NT, Hejazian M, Ooi CH, Kashaninejad N. Recent advances and future perspectives on microfluidic liquid handling. Micromachines. 2017;8(6):186.
31. Nelson G, Kirian RA, Weierstall U, Zatsepin NA, Farago T, Baumbach T, et al. Three-dimensional-printed gas dynamic virtual nozzles for x-ray laser sample delivery. Opt Express. 2016;24(11): 11515–30.
32. Bohne S, Heymann M, Chapman HN, Trieu HK, Bajt S. 3D printed nozzles on a silicon fluidic chip. Rev Sci Instrum. 2019;90(3): 035108.
33. Stagno JR, Liu Y, Bhandari YR, Conrad CE, Panja S, Swain M, et al. Structures of riboswitch RNA reaction states by mix-and-inject XFEL serial crystallography. Nature. 2017;541(7636):242–6.
34. Kupitz C, Olmos JL Jr, Holl M, Tremblay L, Pande K, Pandey S, et al. Structural enzymology using X-ray free electron lasers. Struct Dyn. 2017;4(4):044003.
35. Wang D, Weierstall U, Pollack L, Spence J. Double-focusing mixing jet for XFEL study of chemical kinetics. J Synchrotron Radiat. 2014;21(6):1364–6.
36. Olmos JL Jr, Pandey S, Martin-Garcia JM, Calvey G, Katz A, Knoska J, et al. Enzyme intermediates captured "on the fly" by mix-and-inject serial crystallography. BMC Biol. 2018;16(1):59.
37. Ishigami I, Lewis-Ballester A, Echelmeier A, Brehm G, Zatsepin NA, Grant TD, et al. Snapshot of an oxygen intermediate in the catalytic reaction of cytochrome *c* oxidase. Proc Natl Acad Sci U S A. 2019;116(9):3572–7.
38. Kim D, Echelmeier A, Villarreal JC, Gandhi S, Quintana S, Egatz-Gomez A et al. Electric triggering for enhanced control of droplet generation. Anal Chem. 2019, submitted.
39. Mafune F, Miyajima K, Tono K, Takeda Y, Kohno JY, Miyauchi N, et al. Microcrystal delivery by pulsed liquid droplet for serial femtosecond crystallography. Acta Crystallogr D Struct Biol. 2016;72(4):520–3.
40. Roessler CG, Agarwal R, Allaire M, Alonso-Mori R, Andi B, Bachega JFR, et al. Acoustic injectors for drop-on-demand serial femtosecond crystallography. Structure. 2016;24(4):631–40.
41. Fuller FD, Gul S, Chatterjee R, Burgie ES, Young ID, Lebrette H, et al. Drop-on-demand sample delivery for studying biocatalysts in action at X-ray free-electron lasers. Nat Methods. 2017;14(4):443–9.
42. Weierstall U, James D, Wang C, White TA, Wang D, Liu W, et al. Lipidic cubic phase injector facilitates membrane protein serial femtosecond crystallography. Nat Commun. 2014;5(1):3309.
43. Echelmeier A, Nelson G, Abdallah BG, James D, Roy-Chowdhury S, Tolstikova A, et al. Biphasic droplet-based sample delivery of protein crystals for serial femtosecond crystallography with an x-ray free electron laser. MicroTAS - Int Conf Miniaturized Syst Chem Life Sci. 2015;19:1374–6.
44. Kubo M, Nango E, Tono K, Kimura T, Owada S, Song C, et al. Nanosecond pump-probe device for time-resolved serial femtosecond crystallography developed at SACLA. J Synchrotron Radiat. 2017;24(5):1086–91.
45. Sierra RG, Gati C, Laksmono H, Dao EH, Gul S, Fuller F, et al. Concentric-flow electrokinetic injector enables serial crystallography of ribosome and photosystem II. Nat Methods. 2016;13(1):59–62.
46. Young ID, Ibrahim M, Chatterjee R, Gul S, Fuller F, Koroidov S, et al. Structure of photosystem II and substrate binding at room temperature. Nature. 2016;540(7633):453–7.
47. Ganan-Calvo AM, Montanero JM. Revision of capillary cone-jet physics: electrospray and flow focusing. Phys Rev E Stat Nonlinear Soft Matter Phys. 2009;79(6):066305.
48. Sierra RG, Laksmono H, Kern J, Tran R, Hattne J, Alonso-Mori R, et al. Nanoflow electrospinning serial femtosecond crystallography. Acta Crystallogr D Biol Crystallogr. 2012;68(11):1584–7.
49. Dao EH, Poitevin F, Sierra RG, Gati C, Rao Y, Ciftci HI, et al. Structure of the 30S ribosomal decoding complex at ambient temperature. Rna. 2018;24(12):1667–76.
50. O'Sullivan ME, Poitevin F, Sierra RG, Gati C, Dao EH, Rao Y, et al. Aminoglycoside ribosome interactions reveal novel conformational states at ambient temperature. Nucleic Acids Res. 2018;46(18): 9793–804.
51. Kern J, Alonso-Mori R, Tran R, Hattne J, Gildea RJ, Echols N, et al. Simultaneous femtosecond X-ray spectroscopy and diffraction of photosystem II at room temperature. Science. 2013;340(6131): 491–5.
52. Landau EM, Rosenbusch JP. Lipidic cubic phases: a novel concept for the crystallization of membrane proteins. Proc Natl Acad Sci U S A. 1996;93(25):14532–5.
53. Cherezov V. Lipidic cubic phase technologies for membrane protein structural studies. Curr Opin Struct Biol. 2011;21(4):559–66.
54. Stauch B, Cherezov V. Serial femtosecond crystallography of G protein-coupled receptors. Annu Rev Biophys. 2018;47(1):377–97.
55. Ishchenko A, Gati C, Cherezov V. Structural biology of G protein-coupled receptors: new opportunities from XFELs and cryoEM. Curr Opin Struct Biol. 2018;51:44–52.
56. Sugahara M, Mizohata E, Nango E, Suzuki M, Tanaka T, Masuda T, et al. Grease matrix as a versatile carrier of proteins for serial crystallography. Nat Methods. 2015;12(1):61.
57. Sugahara M, Song C, Suzuki M, Masuda T, Inoue S, Nakane T, et al. Oil-free hyaluronic acid matrix for serial femtosecond crystallography. Sci Rep. 2016;6(1):24484.
58. Conrad CE, Basu S, James D, Wang D, Schaffer A, Roy-Chowdhury S, et al. A novel inert crystal delivery medium for serial femtosecond crystallography. IUCrJ. 2015;2(4):421–30.
59. Park J, Park S, Kim J, Park G, Cho Y, Nam KH. Polyacrylamide injection matrix for serial femtosecond crystallography. Sci Rep. 2019;9(1):2525.
60. Nogly P, Panneels V, Nelson G, Gati C, Kimura T, Milne C, et al. Lipidic cubic phase injector is a viable crystal delivery system for time-resolved serial crystallography. Nat Commun. 2016;7(1): 12314.
61. Nango E, Royant A, Kubo M, Nakane T, Wickstrand C, Kimura T, et al. A three-dimensional movie of structural changes in bacteriorhodopsin. Science. 2016;354(6319):1552–7.
62. Nogly P, Weinert T, James D, Carbajo S, Ozerov D, Furrer A, et al. Retinal isomerization in bacteriorhodopsin captured by a femtosecond x-ray laser. Science. 2018;361(6398):eaat0094.
63. Suga M, Akita F, Sugahara M, Kubo M, Nakajima Y, Nakane T, et al. Light-induced structural changes and the site of O=O bond formation in PSII caught by XFEL. Nature. 2017;543(7643):131–5.
64. Tosha T, Nomura T, Nishida T, Saeki N, Okubayashi K, Yamagiwa R, et al. Capturing an initial intermediate during the P450nor enzymatic reaction using time-resolved XFEL crystallography and caged-substrate. Nat Commun. 2017;8(1):1585.
65. Seibert MM, Ekeberg T, Maia FR, Svenda M, Andreasson J, Jonsson O, et al. Single mimivirus particles intercepted and imaged with an X-ray laser. Nature. 2011;470(7332):78–81.
66. Chavas LM, Gumprecht L, Chapman HN. Possibilities for serial femtosecond crystallography sample delivery at future light sources. Struct Dyn. 2015;2(4):041709.
67. Hantke MF, Hasse D, Maia FRNC, Ekeberg T, John K, Svenda M, et al. High-throughput imaging of heterogeneous cell organelles with an X-ray laser. Nat Photonics. 2014;8(12):943–9.

68. Hantke MF, Hasse D, Ekeberg T, John K, Svenda M, Loh D, et al. A data set from flash X-ray imaging of carboxysomes. Sci Data. 2016;3(1):160061.
69. Kirian RA, Awel S, Eckerskorn N, Fleckenstein H, Wiedorn M, Adriano L, et al. Simple convergent-nozzle aerosol injector for single-particle diffractive imaging with X-ray free-electron lasers. Struct Dyn. 2015;2(4):041717.
70. Awel S, Kirian RA, Wiedorn MO, Beyerlein KR, Roth N, Horke DA, et al. Femtosecond X-ray diffraction from an aerosolized beam of protein nanocrystals. J Appl Crystallogr. 2018;51(1):133–9.
71. Schulz EC, Kaub J, Busse F, Mehrabi P, Muller-Werkmeister HM, Pai EF, et al. Protein crystals IR laser ablated from aqueous solution at high speed retain their diffractive properties: applications in high-speed serial crystallography. J Appl Crystallogr. 2017;50(6):1773–81.
72. Grunbein ML, Nass Kovacs G. Sample delivery for serial crystallography at free-electron lasers and synchrotrons. Acta Crystallogr D Struct Biol. 2019;75(2):178–91.
73. Ghazal A, Lafleur JP, Mortensen K, Kutter JP, Arleth L, Jensen GV. Recent advances in X-ray compatible microfluidics for applications in soft materials and life sciences. Lab Chip. 2016;16(22):4263–95.
74. Murray TD, Lyubimov AY, Ogata CM, Vo H, Uervirojnangkoorn M, Brunger AT, et al. A high-transparency, micro-patternable chip for X-ray diffraction analysis of microcrystals under native growth conditions. Acta Crystallogr D Biol Crystallogr. 2015;71(10):1987–97.
75. Mueller C, Marx A, Epp SW, Zhong Y, Kuo A, Balo AR, et al. Fixed target matrix for femtosecond time-resolved and in situ serial micro-crystallography. Struct Dyn. 2015;2(5):054302.
76. Roedig P, Ginn HM, Pakendorf T, Sutton G, Harlos K, Walter TS, et al. High-speed fixed-target serial virus crystallography. Nat Methods. 2017;14(8):805–10.
77. Lyubimov AY, Murray TD, Koehl A, Araci IE, Uervirojnangkoorn M, Zeldin OB, et al. Capture and X-ray diffraction studies of protein microcrystals in a microfluidic trap array. Acta Crystallogr D Biol Crystallogr. 2015;71(4):928–40.
78. Mathews II, Allison K, Robbins T, Lyubimov AY, Uervirojnangkoorn M, Brunger AT, et al. The conformational flexibility of the acyltransferase from the disorazole polyketide synthase is revealed by an X-ray free-electron laser using a room-temperature sample delivery method for serial crystallography. Biochemistry. 2017;56(36):4751–6.
79. Oghbaey S, Sarracini A, Ginn HM, Pare-Labrosse O, Kuo A, Marx A, et al. Fixed target combined with spectral mapping: approaching 100% hit rates for serial crystallography. Acta Crystallogr Sect D. 2016;72(8):944–55.
80. Daewoong N, Chan K, Yoonhee K, Tomio E, Marcus G-J, Jaehyun P, et al. Fixed target single-shot imaging of nanostructures using thin solid membranes at SACLA. J Phys B Atomic Mol Phys. 2016;49(3):034008.
81. Górzny MŁ, Opara NL, Guzenko VA, Cadarso VJ, Schift H, Li XD, et al. Microfabricated silicon chip as lipid membrane sample holder for serial protein crystallography. Micro and Nano Eng. 2019;3:31–6.
82. Schieferstein JM, Pawate AS, Varel MJ, Guha S, Astrauskaite I, Gennis RB, et al. X-ray transparent microfluidic platforms for membrane protein crystallization with microseeds. Lab Chip. 2018;18(6):944–54.
83. Denz M, Brehm G, Hemonnot CYJ, Spears H, Wittmeier A, Cassini C, et al. Cyclic olefin copolymer as an X-ray compatible material for microfluidic devices. Lab Chip. 2017;18(1):171–8.
84. Doak RB, Nass Kovacs G, Gorel A, Foucar L, Barends TRM, Grunbein ML, et al. Crystallography on a chip - without the chip: sheet-on-sheet sandwich. Acta Crystallogr D Struct Biol. 2018;74(10):1000–7.